journal

J. Am. Ceram. Soc., 83 [8] 2049–54 (2000)

Comparison of Texture Analysis Techniques for Highly Oriented α-Al_2O_3

Matthew M. Seabaugh,*,† Mark D. Vaudin,‡ James P. Cline,*,‡ and Gary L. Messing*

Department of Materials Science and Engineering, Materials Research Laboratory, The Pennsylvania State University, University Park, Pennsylvania 16802

Texture measurements were performed on liquid-phase-sintered alumina textured by a templated grain growth process from 1250° to 1650°C. Texture distributions were measured using X-ray pole figures, rocking curves, Rietveld refinement, and stereology. The March–Dollase equation fitted the measured distributions very well and gave quantitative values of the degree of texture and the texture fraction. The fitting parameters of the X-ray diffraction measurements were comparable to those measured by stereology. Rocking curve analysis was found to be straightforward and to give accurate characterization of texture in the alumina system of this study in a relatively short time.

I. Introduction

The controlled development of texture in polycrystalline materials is a topic of recent interest in ceramic processing, since it allows improved tailoring of physical properties. Physical properties of ceramics that could be tailored by texture control include electrical and thermal conductivity, superconductivity, and magnetic, dielectric, and piezoelectric properties.[1–6] One promising route for controlled texture development is templated grain growth (TGG). In the TGG process, large, anisotropically shaped particles are used as templates for grain growth and are oriented in a fine-particle-size matrix by a shear gradient imposed during forming. During heat treatment, the matrix densifies, and the template particles grow by virtue of their size advantage. The growth of the template grains increases the degree of texture.[7] The starting template concentration, template shape and size, and sintering conditions control texture. The liquid-phase content during grain growth also strongly influences texture development in many systems.[8]

Correlating changes in texture development with processing variables is complex. Each texture measurement technique has strengths and weaknesses, which affect the quality of analysis. Measured texture distributions can be modeled by a variety of equations, but the link between the model equations and processing variables is often weak or absent. Further complications arise from the lack of consensus in the literature on what techniques should be used to measure texture and what parameters should be used to describe the measured distributions. Texture analysis using the simplest techniques, such as relative peak intensity (e.g., Lotgering factor), does not provide information about the distribution of crystal orientations in the material, which can be key in understanding processing–texture relationships.

Based on an evaluation of texture analysis approaches, three X-ray diffraction techniques and a stereological method have been chosen to measure the crystallographic and morphological texture of liquid-phase-sintered alumina specimens prepared by a TGG process. Crystallographic texture reflects the preferred orientation of crystal lattices in the material, and can be measured by the various diffraction techniques, while morphological texture is a measure of the preferred orientation of particle morphology, and is measured stereologically.

The most common method of texture evaluation is pole figure measurement,[9,10] which measures the intensity of a selected X-ray diffraction peak as the sample rotates about two orthogonal axes. To measure axisymmetric textures, typically a diffraction peak from planes normal to the preferred orientation direction is used. This method is widely used for metals and is well suited to measure nonaxisymmetric textures as well. However, pole figure measurements require four-circle goniometers. X-ray rocking curve analysis, with corrections for defocus and X-ray path differences, is another method of texture analysis, and requires only a two-circle powder diffractometer. The intensity of the X-ray diffraction peak from the planes normal to the preferred orientation direction is measured as the sample rotates in θ. This method is generally applicable for measuring axisymmetric texture profiles, and has been applied to bismuth-containing ceramic superconductors,[11] alumina, and thin films of electronic materials and metals.[12] Rietveld refinement of X-ray diffraction data can be used to measure the texture of polycrystalline samples by incorporating a model texture function to describe texture-induced changes in diffraction peak intensities.[13] In this study, the model function used was the March–Dollase equation, which is described below. This technique has been used to characterize texture development in liquid-phase-sintered alumina.[14]

If grain morphology can be uniquely correlated to crystallographic directions or planes, a stereologically determined orientation distribution of anisotropic grains can also be used to quantify texture.[6,15] Other available techniques include orientation imaging microscopy (OIM) that automatically indexes backscattered Kikuchi patterns obtained in the scanning electron microscope, thus providing the means to assess texture on a microscopic scale.[16] In this study, the comparison is confined to stereological measurements and three techniques, pole figures, rocking curves, and Rietveld analysis. The Rietveld refinement and rocking curve techniques are interesting because both use a conventional powder diffractometer. The comparison of the measured texture distributions from these techniques to the more commonly used pole figure measurement provides an evaluation of the strengths and weaknesses of the three methods. In addition, comparison of the diffraction-based results with stereological measurements provides a measure of the correlation between crystallographic and morphological texture.

The specimens in this study were flat sheets with axisymmetric (fiber) texture about the specimen normal (the texture axis). To describe this texture, we specify the preferred crystallographic direction, i.e., the crystal direction preferentially aligned with the texture axis; in this case, the preferred orientation direction is the normal to the alumina basal plane, the [0001] direction. To

K. J. Bowman—contributing editor

Manuscript No. 189105. Received September 9, 1999; approved March 6, 2000.
*Member, American Ceramic Society.
†Now with NexTech Materials, Ltd., Worthington, Ohio 43085.
‡Ceramics Division, National Institute of Standards and Technology, Gaithersburg, Maryland 20899.

quantify the texture, we measured the volume fraction of the specimen whose preferred crystallographic direction was at a given angle to the texture axis. Typically, this volume fraction is divided by the volume fraction of a random specimen at the same angle to give the multiple of a random distribution (MRD). In a diffraction experiment, the intensity of a Bragg peak is proportional to, among other factors, the volume of diffracting material, which makes X-ray diffraction suitable for the measurement of texture in MRDs.

The March–Dollase equation[13] was selected as the model equation to fit to the measured texture (MRD) distributions because its fitting parameters are related to stereologically measurable values. The March equation was first proposed[17] to describe the orientation of anisotropically shaped particles (platelets or rods) in a compact formed by uniaxial pressing. Dollase chose the March equation to adjust for preferred orientation in Rietveld refinements, and extended it to account for microstructures with differently textured components, producing the March–Dollase equation. In this work, we measured the increase of the textured fraction of alumina due to the growth of oriented templates that consume a randomly oriented matrix. Thus, there were two populations of grains in the specimens, one textured, with volume fraction f and texture factor r, and one random. The form of the March–Dollase equation that was used to model the texture in units of MRD for all four techniques was

$$P(f,r,\omega) = f\{r^2 \cos^2 \omega + r^{-1} \sin^2 \omega\}^{-3/2} + (1 - f) \quad (1)$$

For a platelet-containing compact, March defined r as the ratio of the final to initial sample heights during compaction and therefore $0 \leq r \leq 1$. Small r indicates a narrow distribution of platelet normal orientations about the sample normal; r is 1 for a random sample and tends to 0 for a perfectly oriented system. The definitions of r and f remain consistent for all of the techniques, but the definition of ω changes. In Rietveld refinements, ω is the angle between the preferred orientation direction and the normal to the planes whose calculated diffracted intensity is being adjusted for texture. For rocking curve and pole figure measurements, ω is the angle between the specimen normal (texture axis) and the scattering vector, i.e., the specimen tilt angle. For stereological measurements, ω is the angle between the sample normal and the normal to the major facet of the platelet in the cross section.

In a random orientation distribution, the volume of material oriented at ω changes as $\sin \omega$ and therefore the volume fraction for a textured sample is $P(f,r,\omega) \sin \omega$. It can be shown that the normalization condition

$$\int_0^{\pi/2} P(f,r,\omega) \sin \omega \, d\omega = 1 \quad (2)$$

is obeyed. Substituting the limit values of ω (0 and $\pi/2$) into Eq. (1) gives

$$P(r,f,0) = f/r^3 + (1 - f) \quad (3)$$

$$P(r,f,\pi/2) = fr^{3/2} + (1 - f) \quad (4)$$

From Eq. (3), we define $M = 1/r^3$, the MRD of the textured fraction at $\omega = 0$. Equation (4) shows that the MRD profile of a highly textured material (small r) for large values of ω is primarily sensitive to $1 - f$, the volume fraction of unoriented material. We define R as the ratio of the textured to untextured fractions: $R = f/(1 - f)$. If ω_h is the angle at which the MRD falls to half the value at $\omega = 0$, i.e., the half-width at half-maximum (HWHM), then

$$P(r,f,\omega_h) = \frac{f}{2r^3} + \frac{1 - f}{2}$$

For textured samples where $MR \gg 1$, which is the case for all but the most weakly textured samples, solving for $\sin \omega_h$ gives

$$\sin \omega_h = \left\{\frac{4^{1/3} - 1}{M - 1}\right\}^{1/2} = \frac{0.7764}{\sqrt{M - 1}} \quad (5)$$

which is independent of f; note that for small r values, $\omega_h \propto M^{1/2} \propto r^{3/2}$. Another property of Eq. (1) that is of interest is the angle, ω_e, at which the contribution of the textured and random fractions to the texture profile are equal, i.e., $fP(1,r,\omega_e) = 1 - f$. Solving for $\sin \omega_e$ gives

$$\sin \omega_e = \left\{\frac{R^{2/3}/r^2 - 1}{M - 1}\right\}^{1/2} \quad (6)$$

or $\sin \omega_e = R^{1/3} \sqrt{r}$ for small r.

By fitting measurements to a suitable model function that fits the data, properties such as textured fraction and degree of texture can be obtained from Rietveld, rocking curve, pole figure, and stereological measurements. This approach allows fitting parameters, rather than entire orientation profiles to be compared. Since r and f can be measured using both stereological observations and diffraction measurements, correlation between the fitting parameters from all of the techniques employed will show whether the March–Dollase equation is a valid relationship for describing texture–microstructure relationships in this system.

II. Experimental Procedure

(1) Sample Preparation

The samples in this study were liquid-phase-sintered α-Al_2O_3 that was textured by templated grain growth. Liquid phase formers, CaO and SiO_2 (1:1 molar ratio), were added to reduce constrained densification. Such additives also encourage anisotropic grain growth in alumina. The samples used in this study had an initial composition of 95 wt% alumina with 5 wt% glass phase formers, and an initial 5 wt% template loading before sintering. The process for producing the textured samples is described elsewhere.[18]

(2) Rietveld Refinement

The March–Dollase equation (or a similar model texture function) is required for the Rietveld refinement of diffraction data from textured samples. Rietveld refinements were performed with the GSAS Rietveld refinement software package, using a March–Dollase texture profile about the [0001] axis to account for preferred orientation. Powder diffraction data were collected on an X-ray diffractometer equipped with a sample spinner, position-sensitive detector, and focusing incident beam monochromator, which only transmits the Cu$K\alpha_1$ component of the Cu$K\alpha$ doublet. The texture axis was assumed to be normal to the specimen surface, permitting the use of the sample spinner to reduce the effects of particle counting statistics. Data were collected from 20° to 152° 2θ using a scan rate of 1°/min, a total scan time of ~2.25 h. This resulted in the recording of over 60 diffraction peaks of sufficient intensity to be included in the Rietveld refinement. The low-angle limit of 20° was chosen to ensure that constant volume of illumination was met for the refined data. The refinement strategy was similar to that described in Cline *et al.*[14]

(3) Pole Figure Analysis

Pole figure measurements were made using a four-circle diffractometer and Cu$K\alpha$ radiation. Pole figures were measured in steps of $\Delta\omega = 1.5°$ and $\Delta\beta = 36°$ in the ranges of $0° \leq \omega \leq 60°$ and $0° \leq \beta \leq 360°$, with a measuring time of 10 s/point. The ω step was relatively small and the β step relatively large because the specimens typically displayed high levels of axisymmetric texture. An incident slit of 0.5 mm by 3 mm was used, and the samples were oscillated 5 mm during the measurement. The typical data collection time per specimen was 2 h (67 min collection time). The data were averaged over β to produce a distribution of average intensity versus ω. Samples containing no platelets were sintered

under the same conditions as the textured materials to create "random" (or untextured) samples. The measured intensity distribution of the textured sample was divided by the measured intensity distribution from a "random" sample to correct for changes in illumination area with tilt angle, X-ray absorption, and defocus of the beam on the tilted sample and acquire an MRD measurement.

(4) Rocking Curve Method

The rocking curve technique is described in a recent paper.[11] Two X-ray intensity scans were collected using a conventional powder X-ray diffractometer and Cu$K\alpha_1$ radiation. The first was a θ–2θ scan of a Bragg peak (scattering angle $2\theta_B$) diffracted by the basal planes of the alumina; the 000.12 peak was used, $2\theta_B = 90.7°$. The second was a θ scan (rocking curve) with the detector centered on the Bragg peak. Typical data collection time per specimen was 30 min. The scattering angle varies along the length of the specimen when it is tilted out of the symmetric position; this affects the intensity diffracted from different parts of the specimen, and will be referred to as tilt-induced defocusing. (The defocusing that occurs at the symmetric position—the "flat specimen correction"—is insignificant in comparison and can be ignored.) The θ–2θ scan of the Bragg peak gives the variation of scattered intensity with angle and thus it can be used to correct the θ scan intensities for this tilt-induced defocusing.[11,12] The intensity is also corrected for the variation in X-ray absorption with specimen orientation. Since the specimen rotates about the normal to the plane of diffraction, the region of orientation space that can be probed is limited to an ω range of $-\theta_B$ to θ_B at most. Extensive testing on untextured alumina has shown the technique to give accurate results out to ω values near $\pm\theta_B$. The validity of the corrections has been tested extensively as previously described.[11,12] In addition, axisymmetrically textured specimens of various types have produced texture profiles that had mirror symmetry about the line $\omega = 0$, although the date collection process has no such symmetry. Texture profiles recorded from axisymmetrically textured specimens at *N* values of 0° and 90° (rotation about the sample normal) have been found to be essentially identical. Finally, texture profiles obtained from specimens with asymmetric texture at *N* values of 0° and 180° have been accurately related by mirror symmetry about the line $\omega = 0$. The data are processed by TexturePlus, a computer program that implements the defocusing and absorption corrections.[20] These corrections can be viewed as dividing the measured rocking curve intensities by a "random" rocking curve calculated using the θ–2θ scan of the Bragg peak, analogous to the pole figure correction, and so, as discussed above, the corrected intensity profile is proportional to the MRD profile.

(5) Stereological Analysis

After sintering, cross-section specimens normal to the top surface were cut from the textured samples. These specimens were polished, thermally etched for 30 min at 100°C below their sintering temperature, gold-coated, and examined using SEM. Micrographs of sample cross sections were analyzed using image analysis software.[21] The area of each anisotropically shaped grain and its major and minor axis dimensions were tabulated, along with ω, the angle between the major axis and the top surface of the sample. Anisotropic grains were defined as those having an aspect ratio greater than 2.

The orientation distribution of the anisotropic grains was plotted from the measured stereological data. Fitting orientation distribution functions to stereological data has been discussed by Sandlin *et al.*[15] The volume fraction, *f*, of oriented material was determined by measuring the area fraction of anisotropic grains, multiplied by the appropriate stereological correction factor. The *r* value was obtained by determining the distribution of the volume fraction of anisotropic material as a function of ω (using 0.5° bins), and fitting this distribution using the March–Dollase equation (1) with *f* set equal to 1.

III. Results

An example of the highly textured microstructure that results from sintering a specimen for 30 min at 1550°C is shown in Fig. 1; the specimen had a 5% initial template content (initial size: major axis 10–15 μm, and minor axis 1.5–2 μm) with 5% liquid phase formers (equimolar SiO_2:CaO). The texture was measured by stereology and by the three X-ray techniques. For the rocking curve and pole figure methods, the data consisted of the intensity of the 000.12 peak as a function of ω, corrected as described above. For the Rietveld method, the data consisted of the measured intensity for each peak divided by the square of its calculated structure factor; there are two measurements at $\omega = 0$, the 0006 and 000.12 peak intensities, which typically gave different values (discussed below) and the intensity-weighted average of these was used. The March–Dollase equation given in Eq. (1) was fitted to the four sets of data using a nonlinear least-squares method, giving values for *r* and *f*, and also a scale factor which transformed the raw data to the MRD scale. The MRD values for the three X-ray methods are plotted in Fig. 2; Fig. 2(a) shows the angular range $0 < \omega < 25°$ that contains the high MRD values, and Fig. 2(b) shows $15° < \omega < 90°$ at a highly expanded MRD scale. The March–Dollase fits to the data are also plotted. In all cases, the maximum MRD value, *M*, occurs at $\omega = 0$, and as ω increases, the texture profile drops drastically, reaching *M*/10 within 10° of the sample normal, indicating that the volume fraction of material oriented with the [0001] direction normal to the sample surface is many times greater than that of a random specimen. There is a noticeable difference in the widths of the profiles, with the pole figure, rocking curve, and Rietveld profiles being successively narrower.

Table I contains the *r* and *f* values for the three data sets in Fig. 2 and also the results of stereology observations on the same specimens. Also tabulated is the correlation coefficient for the fit of the March–Dollase equation to the data, which is better than 0.9 for all techniques. In the case of the rocking curve it was 0.9997. The table shows that the orientation parameters and textured fractions for all of the methods except pole figure measurements agree well; the pole figure data give a higher *r* value and a lower *f*. From Eq. (5) it was shown that even for low values of *f*, the HWHM of a profile in Fig. 2(a) is proportional to $r^{3/2}$. The *r* values in Table I for pole figure, rocking curve, and Rietveld measurements are successively smaller, which is consistent with the variation in profile widths in Fig. 2(a). The high correlation coefficients for the three diffraction techniques demonstrate the utility of the March–Dollase function.

Apart from the correlation coefficient calculation, no numerical error analysis has been performed on the data. The data in Fig. 2 for the Rietveld and rocking curve techniques are very similar, apart from the MRD value at $\omega = 0$, which is unreliable in the Rietveld case as discussed below. The *r* and *f* values in Table I for

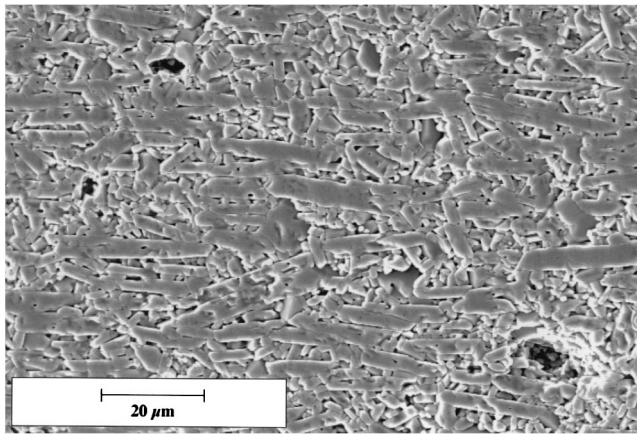

Fig. 1. SEM micrograph of sample with 5% initial template content (initial size: major axis 10–15 μm, minor axis 1.5–2 μm) and 5% liquid phase formers (equimolar SiO_2:CaO), sintered at 1550°C for 30 min.

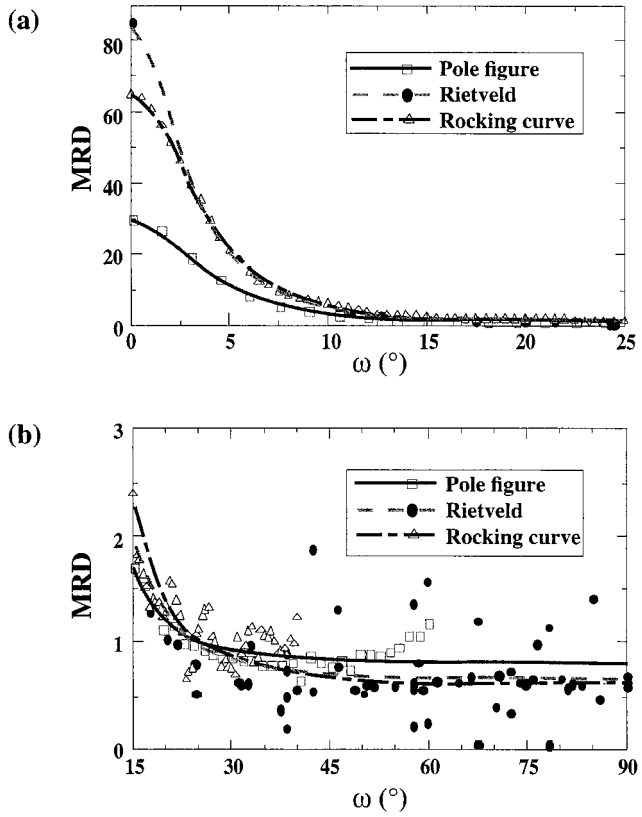

Fig. 2. Pole figure, Rietveld and rocking curve MRD data for TGG alumina sintered 30 min at 1550°C: (a) 0°–20°; (b) 20°–90°. The curves are March–Dollase fits to the data. Note change of MRD scale.

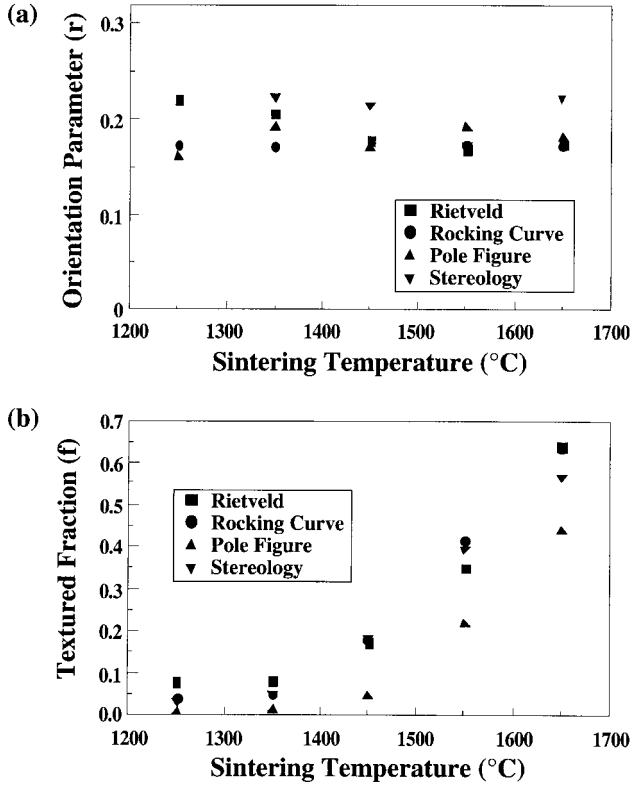

Fig. 3. Comparison of texture parameters for TGG alumina sintered 30 min at various temperatures: (a) orientation parameter (*r*); (b) textured fraction (*f*).

Table I. Parameters of March–Dollase Fit to MRD Profiles from Texture Measurement Techniques

Measurement technique	Orientation parameter (*r*)	Textured fraction (*f*)	Correlation coeff
Rietveld	0.168	0.35	0.990
Rocking curve	0.173	0.41	1.000
Pole figure	0.190	0.21	0.997
Stereology	0.173	0.39	0.953

these methods (and also stereology) are similar and no significance will be attached to differences. The pole figure data, on the other hand, are clearly different at both low and high ω, and the *r* and *f* values in Table I reflect these differences. Therefore, differences of 0.02 in *r* and factors of 2 in *f* will be treated as statistically significant in what follows.

In Fig. 3(a), the *r* parameter from the three X-ray diffraction techniques and the stereological measurements are plotted as a function of sintering temperature. For all techniques, the range of *r* values is 0.16 to 0.225, and *r* is approximately constant throughout the range of heat treatments studied; the stereological results are significantly higher than the diffraction results at three of the four sintering temperatures, and the Rietveld *r* values are higher than the rocking curve and pole figure values at the lower temperatures. The graph in Fig. 3(b) shows the change in textured fraction (*f*) with sintering temperature as measured by the three X-ray diffraction techniques and by stereology. All four techniques indicate that the textured fraction increases as the sintering temperature increases, but that the degree of texture of the oriented fraction remains approximately constant. Considering the *f* values, the agreement between the rocking curve and the stereological measurements is good over the whole temperature range. The initial loading of template grains in these specimens is 5%, and both the rocking curve and stereology results, at 3.6% and 3.2%, respectively, agree fairly well with this value. The Rietveld data agree well with these measurements above 1350°C sintering, but at 1350° and 1250°C the Rietveld results show a higher textured fraction, with 7.6% at 1250°C. The pole figure data give a consistently lower textured fraction throughout. Together, the data in Fig. 3 indicate that with increasing sintering temperature the textured fraction of the sample increased from approximately 5% to at least 50% at a sintering temperature of 1650°C; however, the degree of texture of the textured fraction remained approximately constant, showing that growth of the template grains was the primary mechanism of texture development as reported elsewhere.[18]

IV. Discussion

A large number of data sets were collected in the course of the work on analyzing texture development in templated alumina specimens, and although only a limited number of data sets are presented here for comparison, they are representative of typical behavior observed from many specimens. There are several reasons to choose the March–Dollase equation to model the texture in these materials. The most important is that the equation fits the texture data well; the R^2 values in Table I are all above 0.95. The equation is simple, with only two parameters, and can be applied to different measurement techniques. The equation describes the entire texture distribution, quantifying the fraction of grains at many different orientations, rather than only those perfectly oriented (like a Lötgering factor). Fitting the same equation to all of the techniques allows the fitting parameters for the various techniques to be compared and reveals differences, some of which can be explained by the differences in measurement technique.

We note that stereology is the only direct measure of *f* used in this study, and that the stereological measurement of *r* relies on fitting the measured distribution of orientations. The fact that stereology matches well to diffraction methods implies that March–Dollase analysis of diffraction data (which is an average

over the whole specimen) correlates well with what can be learned about the microstructure of the specimen at the local level by stereology. It should be emphasized that although the agreement in Figs. 3(a) and (b) between the stereological and rocking curve techniques is good over the whole range of sintering temperatures, the comparisons made in this paper are primarily qualitative. To determine definitively the accuracy of any of the texture measurement methods studied, a set of standard materials with a range of known texture parameters must be used to evaluate the methods. The only material of which the authors are aware that has a known texture is SRM676, a standard reference alumina powder that has been shown to produce powder beds that do not display preferred crystallographic orientation. Tests of the rocking curve technique using this powder have given corrected rocking curves of constant intensity, thus validating the technique.[11]

In Fig. 3(a), the agreement in r among the three diffraction methods is good, and the relatively constant value of r for the five samples is consistent for the diffraction and stereological measurements. The higher value of r for the stereological measurement compared to the diffraction-based methods may arise from the differences between morphological and crystallographic texture. In the determination of morphological texture, the orientations of anisotropically shaped grains are measured, and a distribution of volume fraction versus ω is obtained. While this is a valid characterization, experimental error is introduced as a result of the assumptions that all anisotropic grain morphology is strictly a reflection of crystallography, and that the anisotropic grains are the sole source of texture. Anisotropically shaped grains whose shape arises from factors other than crystallography (e.g., by grain accommodation) cannot be separated from the template-shaped grains by SEM observation and are included in the anisotropic (and textured) fraction. The crystallographic orientation of this population is likely more random than the anisotropically shaped grains, thus raising r. It is also possible that texture has developed in the sample matrix, as revealed in several investigations of texture development in commercial alumina substrates.[22] In this case, a fraction of the matrix grains would be crystallographically oriented, but would not have an anisotropic morphology, and therefore would not be included in the morphological analysis. Finally, during sectioning of samples, a number of anisotropic grains in the sample will be cut such that they present an isotropic cross section. These grains will not be counted in the measurement of the anisotropic fraction. As previously stated, in the stereological analysis, grains with an aspect ratio ≥ 2 in the 2-D section were counted as anisotropic grains. For grains with an aspect ratio ≥ 5 (the lowest observed aspect ratio in this study was ~ 6), the underestimation of the anisotropic fraction because of sectioning (i.e., the fraction of sections with an aspect ratio <2 which can be cut from a disk with aspect ratio of 5) can be geometrically calculated to be less than 3%. Together these considerations reveal that the stereological technique slightly underestimates the volume fraction of template grains and presents a wider distribution of grain orientation.

The effect of an untextured fraction on Eq. (1) is to give a positive offset to the MRD distribution, which becomes a more significant fraction of the total MRD at higher ω values where the intensity from the textured fraction decreases. Equation (6) shows that for highly textured specimens with r values of 0.2, the random contribution component to the MRD profile becomes larger than that of the textured component above $\omega_e = \sin^{-1}(0.447R^{1/3})$, which gives $\omega_e \approx 15°$ for $f = 0.2$ and $\omega_e \approx 18°$ for $f = 0.25$. We define two angle regions for ω, a low-angle region below ω_e and a high-angle region above. The MRD values in the high ω region of a texture profile are dominated by the random component, and we see a correlation between larger MRD values at high ω in Fig. 2(b) and smaller f values in Table I.

Differences in the f value measured by the diffraction techniques (Fig. 3(b)) may be traceable to experimental differences. In particular, the sampling frequency and range are different. The rocking curve method has the smallest ω measurement range ($-40° < \omega < 40°$), but also the smallest sampling interval in ω (step size of 0.2°). The pole figure measurement has a larger ω step size of 1.5°, and a larger range of measurement ($0 < \omega < 60°$). The Rietveld refinement includes intensities over the entire range of ω, from 0° to 90°, but the number of data points in the low ω region is small. All three techniques collect data in both the low- and high-angle regions, with data from the pole figure and rocking curve methods being fairly evenly split between the two regions and the Rietveld method using predominantly high ω data. Since the data which are most sensitive to f (data above ω_e) are of low intensity and more subject to random and systematic errors, particular with respect to noise and background subtraction, we would expect that accurate measurement of the textured fraction, i.e., the f parameter, would be more challenging than the measurement of r. Nonetheless, the data for f in Fig. 3(b) are very consistent, with the most obvious difference being the lower f value determined from pole figure measurements across the whole temperature range.

The raw intensity distribution of the measured pole figures and rocking curves must be corrected for geometric considerations, namely X-ray absorption and defocus of the beam on a tilted sample.[10,11] The intensity measured by the rocking curve method is corrected using a high-resolution scan of the 000.12 peak, as detailed by Vaudin *et al.*[11] The pole figure samples were corrected for the same considerations by dividing the measured intensity by the intensity from a "random" sample. While the "random" samples have the correct amount of liquid phase and densities and grain sizes similar to those of the textured materials, they may be slightly textured, as has been demonstrated for several substrate materials.[22] Examination of the "random" samples by Rietveld methods, and also by rocking curve analysis using $11\bar{2}3$, $11\bar{2}6$, and $30\bar{3}0$ peaks, revealed minimal texture out to the angles accessible by the rocking curve technique, but as demonstrated by Böcker *et al.*[23] evaluation of weak basal plane texture in alumina can require pole figure measurements of several peaks, because the intensities of basal plane peaks from alumina (0006 and 000.12) are intrinsically weak. The textured alumina specimens in this study produced 000.12 peaks of significant intensity, so that a single pole figure was adequate for measuring axisymmetric texture about the (0001) pole; however, the 000.12 intensity from the "random" specimen was very low, making the pole figure correction factor susceptible to noise and background errors, as discussed above. Figure 3(b) shows that at all of the sintering temperatures, the f values for the textured samples measured by the pole figure technique are lower than those for all of the other techniques across the whole range of sintering temperatures. This systematic difference may be attributable to weak texture in the "random" samples. If the "random" specimen were weakly textured, the intensity from the "random" specimen at high ω values would be decreased below what a truly random specimen would give, and therefore the MRD would be systematically increased at high ω values, which in turn would reduce the textured fraction measured for the templated samples. The gradual increase in the rocking curve texture profile above $\omega = 40°$ in Fig. 2(b) suggests that the intensity from the "random" sample is decreasing in this angle range while the intensity from the textured specimen is remaining relatively constant.

The number of observable peaks in the diffraction patterns used in the Rietveld refinement technique (65) is controlled by the structure factor of the material and the wavelength of the X-radiation. For X-ray diffraction from alumina using Cu$K\alpha_1$ radiation, after the two data points at $\omega = 0$ (the 0006 and 000.12 peaks), the peak with the next lowest ω value is at 11.13° (the 101.16 peak). There is a lack of data points between 0° and 10°, the ω region in which more than 90% of the decrease in measured intensity in the texture measurements occurs (see Fig. 2). For rocking curves and pole figures, the shape of the curve in the low-ω region principally determines the value of r, but for the Rietveld analysis, the r and f values are principally determined by the ω range with the highest density of relatively intense data points, which is above 10°. An additional problem is the discrepancy between the intensity of the basal peaks, 0006 and 000.12. These peaks are <1% and 4% of the maximum peak intensity for random alumina, respectively, and there was typically a wide

disparity, a factor of 2 or more, in the MRD values obtained from these two peaks. Attempts to reconcile these data by including extinction coefficients in the refinement did not significantly improve the fit or reconcile the two basal peak intensities. The cause of this discrepancy remains unresolved. Despite these concerns, the Rietveld results match well to the stereology and rocking curves, except at low sintering temperatures.

In many ways the rocking curve and Rietveld are complementary techniques with respect to the angular ranges of data that they can collect in this materials system. In contrast to the Rietveld refinement technique, the rocking curve data points can be at as high an ω density as the user requires, but the upper limit of ω that can be accessed is limited to a few degrees less than the Bragg angle of the peak being measured (45.35° in this case). For all of the methods studied, measurements of r and f require that the March–Dollase function provides a good fit, and the fit to the rocking curve data was typically better than the fit of the other techniques. The good fit of the rocking curve data up to $\omega = 40°$ compensated for the lack of data above 40° and added credibility to the r and f values derived. The speed of data collection and analysis can be an issue when the rocking curve has the shortest total data collection of the methods, typically about 30 min. One reason for the faster data collection time for rocking curves in comparison to pole figures is that the X-ray footprint is ~10 mm × 5 mm, much larger than the 0.5 mm × 3 mm for pole figures. This has the added advantage that rocking curves can be used to collect texture data from weakly diffracting specimens such as thin films, with thicknesses down to 20 nm. However, the rocking curve technique is not well-suited to characterizing specimens with weak texture where the texture profile has significant intensity beyond the ω range that can be measured. For such specimens, the Rietveld method has an advantage in that it employs data over the whole ω range; however, for specimens with high symmetry (unlike alumina), the small number of peaks excited by the Cu$K\alpha$ radiation may be insufficient for an accurate texture measurement.

V. Summary

The March–Dollase equation is a relatively simple model that accurately describes texture distributions in TGG alumina. The fit of the March–Dollase equation to measured texture distributions is excellent for a variety of X-ray diffraction techniques, and the agreement of fitting parameters among the XRD techniques is also good. Most importantly, the parameters of the March–Dollase equation are related to physical properties of the microstructure and show good agreement with stereologically measured values.

The data obtained by rocking curve texture measurement are similar to those by other techniques. Additionally, the rocking curve measurements can be performed using a two-circle diffractometer. The simplicity and speed of measurement and analysis, the previously reported validation of the technique using untextured alumina powder, and agreement with other techniques make the rocking curve analysis a good choice for straightforward texture measurement for axisymmetric ceramic materials with significant texture. In order to go beyond technique comparisons and determine the accuracy of the texture measurement methods studied in this paper, it will be necessary to devise a set of standard materials with a range of known textures.

References

[1] G. E. Youngblood and R. S. Gordon, "Texture–Conductivity Relationships in Polycrystalline Lithia-Stabilized β″-Alumina," *Ceram. Int.*, **4** [3] 93–98 (1978).

[2] D. P. Norton, A. Goyal, J. D. Budai, D. K. Christen, D. M. Kroeger, E. D. Specht, Q. He, B. Saffian, M. Paranthaman, C. E. Klabunde, D. F. Lee, B. C. Sales, and F. A. List, "Epitaxial $YBa_2Cu_3O_7$ on Biaxially Textured Nickel (001): An Approach to Superconducting Tapes with High Critical Current Density," *Science*, **274**, 755–57 (1996).

[3] H. Stäblein and J. Willbrand, "Changes in Crystal Texture of Barium Ferrite on Sintering," *IEEE Trans. Mag.*, **2** [3] 459–63 (1966).

[4] S. Swartz, W. A. Schulze, and J. A. Biggers, "Fabrication and Electrical Properties of Grain Oriented $Bi_4Ti_3O_{12}$ Ceramics," *Ferroelectrics*, **38**, 765–68 (1981).

[5] B. Brahmaroutu, G. L. Messing, S. Trolier-McKinstry, and U. Selvaraj, "Templated Grain Growth of Textured $Sr_2Nb_2O_7$"; pp. 883–86 in *ISAF '96 Proceedings of the 10th IEEE International Symposium on Applications of Ferroelectrics*, Vol. 2. Edited by B. M. Kulwicki, A. Amin, and A. Safari. Institute of Electrical and Electronics Engineers, Piscataway, NJ, 1996.

[6] H. J. Bunge, "Textures in Nonmetallic Materials," *Textures Microstruct.*, **14–18**, 283–326 (1991).

[7] M. M. Seabaugh, I. H. Kerscht, and G. L. Messing, "Texture Development by Templated Grain Growth in Liquid-Phase-Sintered α-Alumina," *J. Am. Ceram. Soc.*, **80** [5] 1181–88 (1997).

[8] M. M. Seabaugh, S.-H. Hong, I. H. Kerscht, and G. L. Messing, *Ceramic Microstructure: Control at the Atomic Level*; pp. 303–10. Edited by A. P. Tomsia and A. Glaeser. Plenum Press, New York, 1998.

[9] Y. Ma and K. J. Bowman, "Texture in Hot Pressed or Forged Alumina," *J. Am. Ceram. Soc.*, **74** [11] 2941–44 (1991).

[10] H. J. Bunge, "Experimental Techniques"; Ch. 3 in *Quantitative Texture Analysis*. Edited by H. J. Bunge and C. Esling. DGM Informationsgesellschaft m.b.H., Oberursel, Germany, 1986.

[11] M. D. Vaudin, M. W. Rupich, M. Jowett, G. N. Riley Jr., and J. F. Bingert, "A Method for Crystallographic Texture Investigation Using Standard X-ray Equipment," *J. Mater. Res.*, **13** [10] 2910–19 (1998).

[12] M. D. Vaudin, "Accurate Texture Measurements on Thin Films Using a Powder X-ray Diffractometer"; pp. 186–91 in *ICOTOM-12, Proceedings of the 12th International Conference on Textures of Materials*. Edited by J. A. Szpunar. NRC Research Press, Ottawa, Canada, 1999.

[13] W. A. Dollase, "Correction of Intensities for Preferred Orientation in Powder Diffractometry: Application of the March Model," *J. Appl. Crystallogr.*, **19**, 267–72 (1986).

[14] J. P. Cline, M. D. Vaudin, J. E. Blendell, C. A. Handwerker, R. Jiggetts, K. J. Bowman, and N. Mendendorp, "Texture Measurement of Sintered Alumina Using the March–Dollase Function"; pp. 473–78 in *Advances in X-ray Analysis*, Vol. 37. Edited by J. V. Gilfrich, C. C. Goldsmith, T. C. Huang, R. Jenkins, and I. C. Noyan. Plenum Press, New York, 1994.

[15] M. S. Sandlin, C. R. Peterson, and K. J. Bowman, "Texture Measurement on Materials Containing Platelets Using Stereology," *J. Am. Ceram. Soc.*, **77** [8] 2127–31 (1994).

[16] B. L. Adams, S. Wright, and K. Kunze, "Orientation Imaging: The Emergence of a New Microscopy," *Metall. Trans. A*, **24A**, 819 (1993).

[17] A. March, "Mathematische Theorie der Regelung nach der Korgestalt bei Affiner Deformation," *Z. Kristallogr.*, **81**, 285–97 (1932).

[18] M. M. Seabaugh, G. L. Messing, and M. D. Vaudin, "Texture Development and Microstructure Evolution in Liquid-Phase-Sintered α-Al_2O_3 Ceramics Prepared by Templated Grain Growth," *J. Am. Ceram. Soc.*, submitted for publication.

[19] A. Larson and R. Von Dreele, General Structure Analysis System, Los Alamos National Laboratory, Los Alamos, NM.

[20] M. D. Vaudin, TexturePlus, Ceramics Division, National Institute of Standards and Technology, Gaithersburg, MD 20899-8522. Program available on the Web: http://www.ceramics.nist.gov/staff/vaudin.htm. Also on written request: E-mail: mark.vaudin@nist.gov; fax: (301) 775-5334.

[21] W. Rasband, NIH Image, v. 1.56, National Institutes of Health, Gaithersburg, MD.

[22] J. Huber, W. Krahn, J. Ernst, A. Böcker, and H. J. Bunge, "Texture Formation in Al_2O_3 Substrates," *Mater. Sci. Forum*, **157–162**, 1411–16 (1994).

[23] A. Böcker, H. G. Brokmeier, and H. J. Bunge, "Determination of Preferred Orientation Textures in Al_2O_3 Ceramics," *Eur. Ceram. Soc.*, **8**, 187–94 (1991). □